PERGAMON

International Journal of Solids and Structures 40 (2003) 4167–4180

INTERNATIONAL JOURNAL OF SOLIDS and STRUCTURES

www.elsevier.com/locate/ijsolstr

Sensitivity analysis of the thermomechanical response of welded joints

J. Song [a], J. Peters [b], A. Noor [b,c,*], P. Michaleris [a]

[a] *Department of Mechanical and Nuclear Engineering, 232 Reber Building, Pennsylvania State University, University Park, PA 16802, USA*

[b] *Center for Advanced Engineering Environments, Old Dominion University, MS 201 NASA, Langley Research Center, Hampton, VA 23681, USA*

[c] *University of Florida, Gainesville, USA*

Received 10 February 2003

Abstract

A computational procedure is presented for evaluating the sensitivity coefficients of the thermomechanical response of welded structures. Uncoupled thermomechanical analysis, with transient thermal analysis and quasi-static mechanical analysis, is performed. A rate independent, small deformation thermo-elasto-plastic material model with temperature-dependent material properties is adopted in the study. The temperature field is assumed to be independent of the stresses and strains. The heat transfer equations emanating from a finite element semi-discretization are integrated using an implicit backward difference scheme to generate the time history of the temperatures. The mechanical response during welding is then calculated by solving a generalized plane strain problem. First- and second-order sensitivity coefficients of the thermal and mechanical response quantities (derivatives with respect to various thermomechanical parameters) are evaluated using a direct differentiation approach in conjunction with an automatic differentiation software facility. Numerical results are presented for a double fillet conventional welding of a stiffener and a base plate made of stainless steel AL-6XN material. Time histories of the response and sensitivity coefficients, and their spatial distributions at selected times are presented.

Keywords: Welding; Finite element analysis; Thermal analysis; Lagrangian frame; Residual stresses; Sensitivity analysis

1. Introduction

Welding has become a prevalent mechanical joining methodology in various industries because of its many advantages over other joining methods including design flexibility, cost savings, reduced overall weight, and enhanced structural performance. However, the local high temperature in a welding process

* Corresponding author. Address: Center for Advanced Engineering Environments, Old Dominion University, MS 201 NASA, Langley Research Center, Hampton, VA 23681, USA. Tel.: +1-757-864-1989/1978; fax: +1-757-864-8089.

E-mail address: a.k.noor@larc.nasa.gov (A. Noor).

0020-7683/03/$ - see front matter © 2003 Elsevier Science Ltd. All rights reserved.
doi:10.1016/S0020-7683(03)00223-3

induces residual stresses and distortions (Gunnert, 1955; Terai, 1978; Shim et al., 1992; Connor, 1987). These residual stresses and distortions are undesirable in general since they have bad effects on the structural performance. Although a number of approaches have been proposed to minimize the residual stresses and distortions, including selecting the type of welding, controlling the welding process parameters, and modifying the structural configuration (Burak et al., 1977, 1979), the residual stresses are inevitable in essence.

Numerical simulation techniques to study the various phenomena associated with welding have been developed. For example, weld-pool physics, heat and fluid flow, heat source–metal interactions, weld solidification microstructures, phase transformations, and residual stresses and distortions have been studied. Recent studies of residual stresses and distortions in welded structures are reported in Goldak and Bibby (1988), Tekriwal and Mazumder (1991), Argyris et al. (1982), Hibbitt and Marcal (1973), Braudel et al. (1986), Oddy and Goldak (1990), Bertram and Ortega (1991), Wang and Murakawa (1998), Roelens and Maltrud (1993), Rybicki and Stonesifer (1979) and Chakravati et al. (1986). In these numerical studies of welding, the accuracy of temperature-dependent material properties plays an important role in the accuracy of predicted residual stresses.

Since current measurement technology does not allow the accurate determination of the material parameters that are used in the analytical models, it is useful to assess the sensitivity of the thermomechanical responses of welded joints to variations in the various material parameters. The present study focuses on this topic. Specifically, the objective of this paper is to present a computational procedure for evaluating the sensitivity coefficients of the quasi-static response of welded joints. Uncoupled thermomechanical analysis is performed. A rate independent, small deformation thermo-elasto-plastic material model with temperature-dependent material properties is adopted.

Numerical results are presented for the temperature—and residual stress—time histories and their sensitivity coefficients for a double fillet conventional welding of a stiffener and a base plate made of stainless steel AL-6XN. A two-dimensional generalized plane strain model is used, which is adequate for predicting the residual stresses. However, the prediction of welding distortions requires a global three-dimensional model (Brown and Song, 1992), which is beyond the scope of the present study.

2. Finite element equations

Uncoupled thermomechanical analysis is performed. The temperature field is assumed to be independent of stresses and strains. The heat transfer equations emanating from a finite element semi-discretization are integrated using an implicit backward difference scheme to generate the time history of the temperatures. The mechanical response during welding is then calculated by solving a generalized plane strain problem. A rate independent, small deformation thermo-elasto-plastic material model with temperature-dependent material properties is adopted in the study. The governing equations for the thermal and mechanical analyses are summarized subsequently.

2.1. Thermal analysis

The governing equation for transient heat transfer analysis is given by:

$$\rho c_p \frac{\mathrm{d}T}{\mathrm{d}t}(\mathbf{r},t) = -\nabla \cdot \mathbf{q}(\mathbf{r},t) + Q(\mathbf{r},t) \tag{1}$$

where ρ is the density of the flowing body, c_p is the specific heat capacity, T is the temperature, $\mathbf{q}$ is the heat flux vector, Q is the internal heat generation rate, t is the time, $\mathbf{r}$ is the coordinate in the reference configuration, and ∇ is the spatial gradient operator.

The nonlinear isotropic Fourier heat flux constitutive relation is used:

$$\mathbf{q} = -\mathbf{k}\nabla T \tag{2}$$

where $\mathbf{k}$ is the temperature-dependent thermal conductivity.

The rate of internal heat generation by the welding torch is modeled with a "double ellipsoidal" power density distribution proposed by Goldak et al. (1984), and is described by the following equation:

$$Q = \frac{6\sqrt{3}Q_{\mathrm{w}}\eta_{\mathrm{w}}f}{abc\pi\sqrt{\pi}} \exp\left(-\left[\frac{3x^2}{a^2} + \frac{3y^2}{b^2} + \frac{3z^2}{c^2}\right]\right) \ [\mathrm{W/mm^3}] \tag{3}$$

where Q_{w} (2680.35 W/mm^3) is the welding heat input; η_{w} (1.0) is the welding efficiency, x, y, and z are the local coordinates of the double ellipsoid model aligned with the weld fillet; a ($5\sqrt{2}$ mm) is the weld width; b ($5\sqrt{2}$ mm) is the weld penetration; c is the weld ellipsoid length ($c = a$ and $f = 0.6$ before the torch passes the analysis region, and $c = 4a$ and $f = 1.4$ after the torch passes the analysis region); v (6.35 mm/s) is the welding torch speed. The numbers in the parentheses are the values which are used in the present study.

The initial temperature field is given by

$$T = {}^0T \quad \text{in the entire volume } V \tag{4}$$

where ${}^0T$ is the prescribed initial temperature. The following boundary conditions are applied on the surface:

$$T = \bar{T} \quad \text{on the surface } A^T, \text{ with prescribed temperatures} \tag{5}$$

$$q = \bar{q} \quad \text{on the surface } A^q, \text{ with prescribed heat fluxes} \tag{6}$$

where $\bar{T}$ and $\bar{q}$ represent the prescribed temperature and temperature-dependent surface flux, respectively.

The application of finite element discretization in conjunction with a weak formulation of the problem yields the element residual vector $\mathbf{R}$ as follows:

$$\mathbf{R}({}^n\mathbf{T}) = \sum_V \left\{ \mathbf{B}^{\mathrm{T}}\mathbf{k}\mathbf{B}\,{}^n\mathbf{T} - \mathbf{N}^{\mathrm{T}}Q + \mathbf{N}^{\mathrm{T}}\mathbf{N}\rho C_p \frac{{}^n\mathbf{T} - {}^{n-1}\mathbf{T}}{{}^nt - {}^{n-1}t} \right\} WJ + \sum_{A_q} \mathbf{N}^{\mathrm{T}}\bar{q}wj \tag{7}$$

where the left superscripts $(n-1)$ and n refer to the time increments ${}^{n-1}t$ and ${}^nt$, $\mathbf{T}$ is element nodal temperature vector, $\mathbf{N}$ and $\mathbf{B}$ are the usual matrices which interpolate the temperature T and temperature gradient ∇T in an element; J and j are the volume and area Jacobian component corresponding to the weight coefficients W and w of the Gaussian quadrature formulas for volume and surface integration.

2.2. Mechanical analysis

The stress equilibrium equation in the Lagrangian frame is given by:

$$\nabla \cdot \mathbf{S} + \mathbf{b} = 0 \quad \text{in } V \tag{8}$$

where $\mathbf{S}$ is the second-order stress tensor, and $\mathbf{b}$ is the body force vector. The boundary conditions are:

$$\mathbf{u} = \bar{\mathbf{u}} \quad \text{on surface } A^u \tag{9}$$

$$\mathbf{S}\mathbf{n} = \bar{\mathbf{t}} \quad \text{on surface } A^t \tag{10}$$

where $\bar{\mathbf{u}}$ is the prescribed displacement vector on surface A^u, $\bar{\mathbf{t}}$ is the prescribed traction vector on surface A^t, and $\mathbf{n}$ is the unit outward normal to the surface A^t. The total strain is the Green's strain:

$$\mathbf{E} = \frac{1}{2}\{\nabla\mathbf{u} + [\nabla\mathbf{u}]^{\mathrm{T}}\} \tag{11}$$

Because of the symmetry, the stress tensor **S** and strain tensor **E** are commonly represented by the vectors $\boldsymbol{\sigma}$ and $\boldsymbol{\epsilon}$ (usually called engineering stress and strain) for computational efficiency. The initial conditions are:

$$\mathbf{u} = {}^{0}\mathbf{u} \tag{12}$$

$$\boldsymbol{\epsilon}_{\mathrm{p}} = {}^{0}\boldsymbol{\epsilon}_{\mathrm{p}} \tag{13}$$

$$\epsilon_q = {}^{0}\epsilon_q \tag{14}$$

where $\boldsymbol{\epsilon}_{\mathrm{p}}$ is the plastic strain vector and ϵ_q is the equivalent plastic strain.

Assuming small deformation thermo-elasto-plasticity, the total strain vector $\boldsymbol{\epsilon}$ is decomposed into the elastic strain vector $\boldsymbol{\epsilon}_{\mathrm{e}}$, the plastic strain vector $\boldsymbol{\epsilon}_{\mathrm{p}}$ and thermal strain vector $\boldsymbol{\epsilon}_{\mathrm{t}}$:

$$\boldsymbol{\epsilon} = \boldsymbol{\epsilon}_{\mathrm{e}} + \boldsymbol{\epsilon}_{\mathrm{p}} + \boldsymbol{\epsilon}_{\mathrm{t}} \tag{15}$$

The stress–strain relationship is:

$$\boldsymbol{\sigma} = \mathbf{C}\boldsymbol{\epsilon}_{\mathrm{e}} = \mathbf{C}[\boldsymbol{\epsilon} - \boldsymbol{\epsilon}_{\mathrm{p}} - \boldsymbol{\epsilon}_{\mathrm{t}}] \tag{16}$$

where **C** is the temperature-dependent material stiffness tensor.

A generalized plane strain condition is assumed to account for the out-of-plane expansion in the model. The out-of-plane strain ϵ_z is assumed to have a linear distribution over the analysis plane:

$$\epsilon_z = e - x\phi_y + y\phi_x \tag{17}$$

where e is the out-of-plane strain at the origin of the coordinate system and ϕ_x and ϕ_y are the strain variations in the y and x directions, respectively.

Similarly to the thermal analysis, the application of the finite element discretization in conjunction with a weak formulation yields the element residual **R** (see, for example, Simo and Taylor, 1985; Tekriwal and

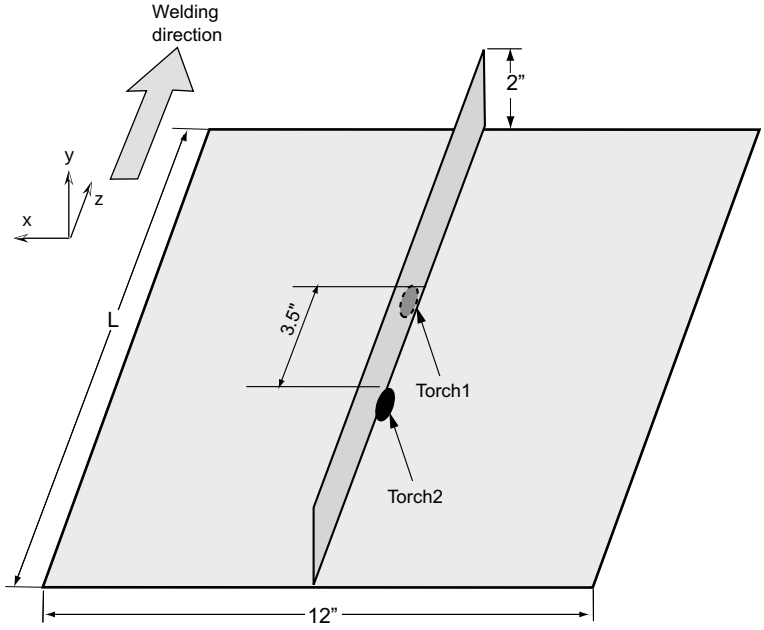

Fig. 1. Welding conditions for double fillet welding.

Mazumder, 1991; Argyris et al., 1982; Hibbitt and Marcal, 1973; Braudel et al., 1986; Michaleris et al., 1995; Rybicki and Stonesifer, 1979; Shim et al., 1992; Bertram and Ortega, 1991).

$$\mathbf{R}({}^{n}\mathbf{U}) = \sum_{V}[\mathbf{B}^{\mathrm{T}}{}^{n}\boldsymbol{\sigma} - \mathbf{N}^{\mathrm{T}}\mathbf{b}]WJ - \sum_{A^t}\mathbf{N}^{\mathrm{T}}\bar{\mathbf{t}}wj \tag{18}$$

where

$${}^{n}\boldsymbol{\sigma} = {}^{n-1}\boldsymbol{\sigma} + \Delta\boldsymbol{\sigma} \tag{19}$$

3. Sensitivity analysis

The sensitivity coefficients, which are the derivatives of the various thermal and mechanical response quantities with respect to the material parameters, are evaluated by using the direct differentiation method in conjunction with the automatic differentiation software facility ADIFOR (Carle et al., 1998; Bischof et al., 1996, 1992). The sensitivity coefficients obtained by ADIFOR were validated by comparing them with those obtained by finite difference approximations. The sensitivity information can be used to (see, for example Saltelli et al., 2000): (a) assess the importance of the parameters used in describing the thermal and mechanical properties of the material on the time histories of the temperature and residual stresses. This,

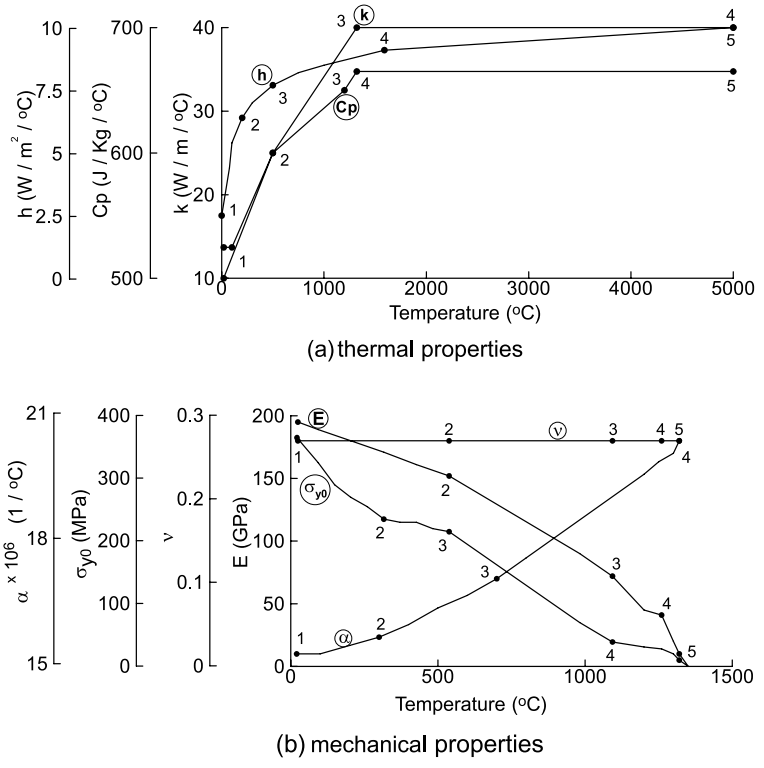

Fig. 2. Temperature-dependent thermal and mechanical properties for AL-6XN: (a) conductivity k, specific heat c_p, and convection coefficient h; (b) elastic modulus E, yield strength σ_y, Poisson's ratio v, and thermal expansion coefficient α.

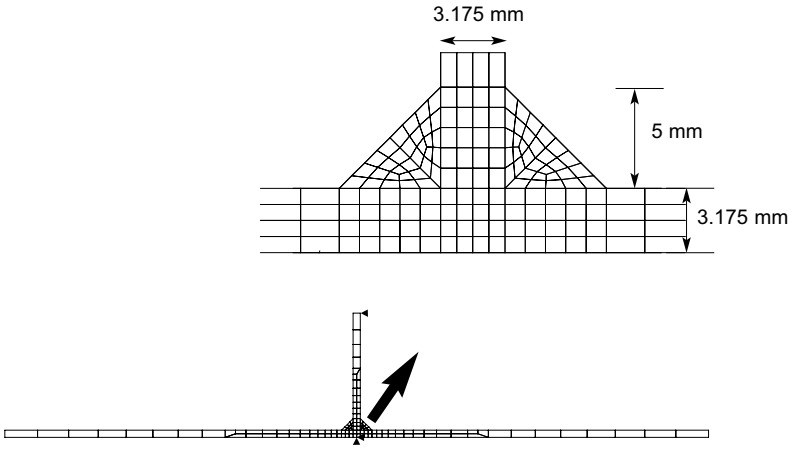

Fig. 3. 2D Lagrangian analysis model.

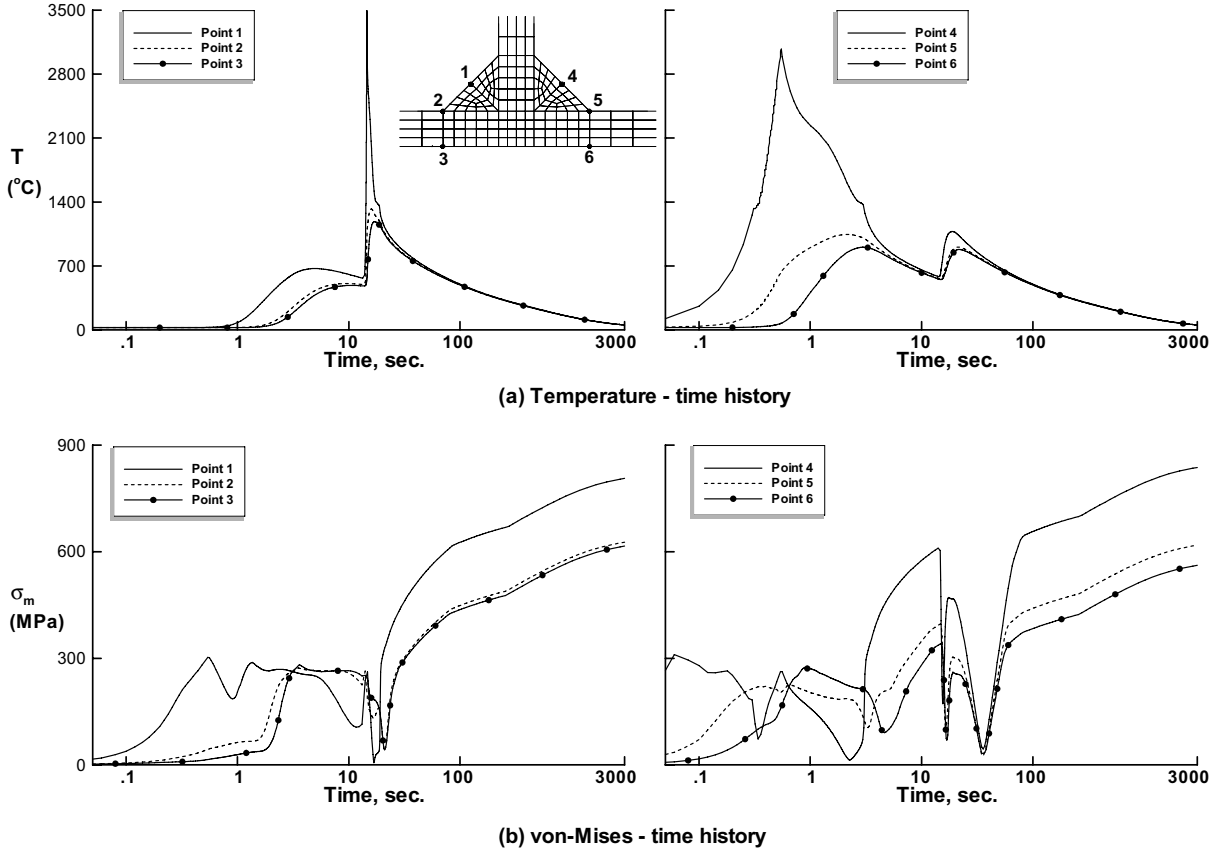

Fig. 4. Time histories of the temperature and von-Mises stress for the welded joint shown in Fig. 1.

in turn, can help both in refining the material models and in the design of improved materials; (b) assess the effects of uncertainties in the material parameters on the time-history response of welded structures; and (c) predict the changes in the time-history response of welded structures due to changes in the material parameters.

4. Numerical studies

The computational procedure described in the preceding sections is applied to study the temperature and residual stress-time histories and their sensitivity coefficients for a double fillet conventional welding of a stiffener and a base plate made of stainless steel AL-6XN (see Fig. 1). The variations of the thermal and mechanical properties of AL-6XN with temperature are shown in Fig. 2. Each of the thermal and mechanical properties is approximated by the piecewise linear variation shown in Fig. 2.

4.1. Welding process and welding conditions

The schematic welding configuration used in the present study is shown in Fig. 1. The width (B) of the base plate is 12 in., the height of the stiffener is 2 in. and the thickness of each of the base plate and stiffener is 1/8 in.

Double fillet welding is used with one welding gun on either side of the stiffener. The guns are 3.5 in. offset from each other with one gun following the other as shown in Fig. 1. The details of the welding process and welding conditions are described in Deo and Michaleris (2003).

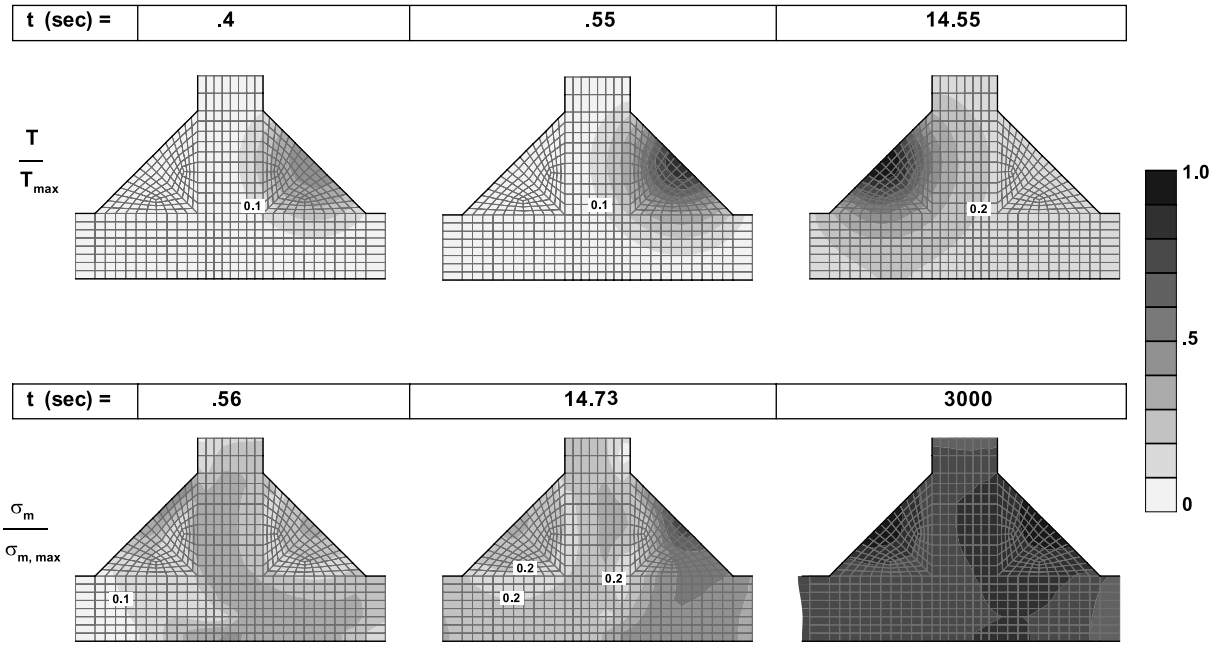

Fig. 5. Snapshots of the normalized temperature and von-Mises stress for the welded joint shown in Fig. 1.

4.2. Finite element model

The finite element model used in each of the thermal and mechanical analyses is shown in Fig. 3. The model has 388 8-node quadratic elements and 1343 nodes. In the thermal analysis all the free surfaces are

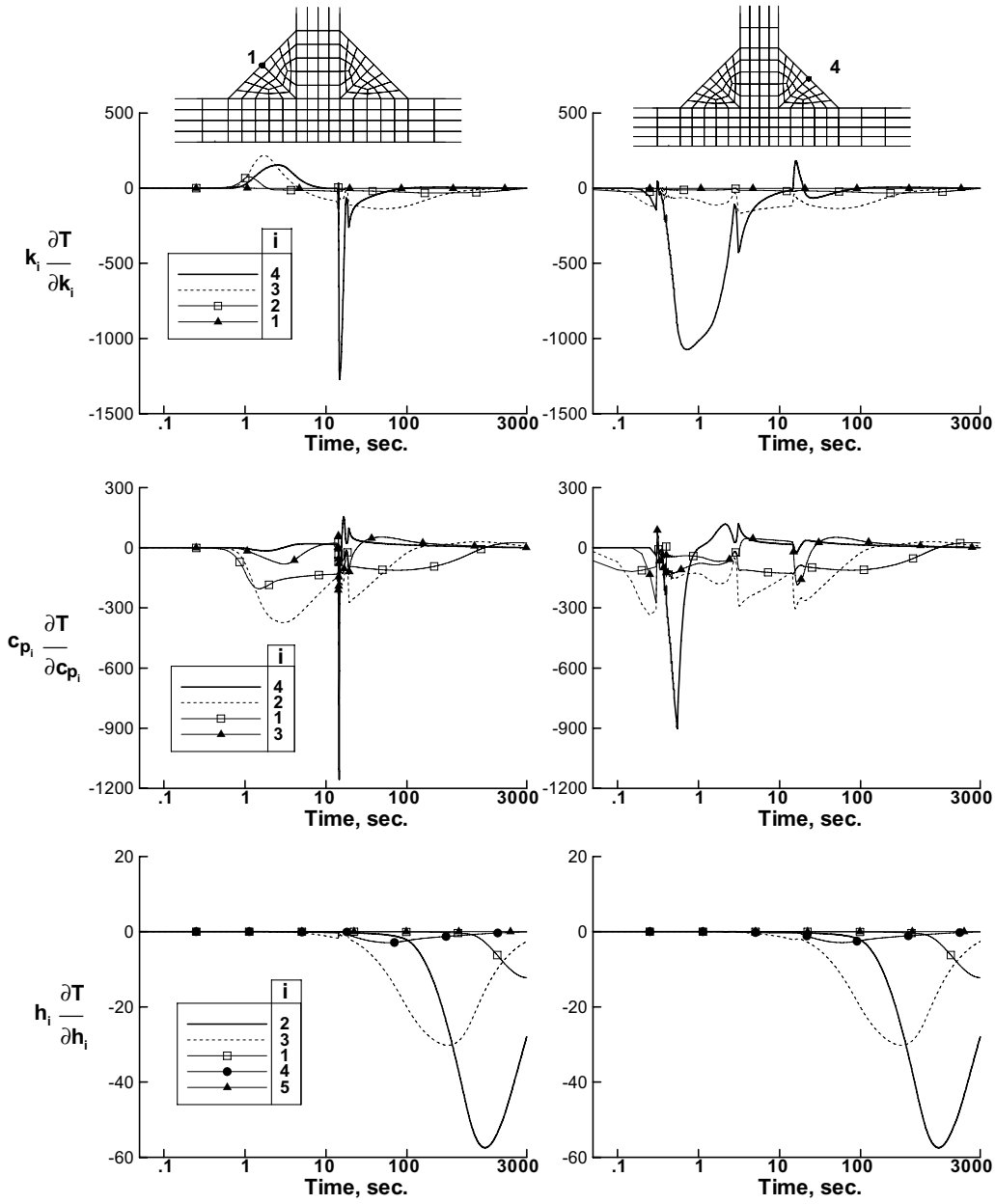

Fig. 6. Time histories of the first-order sensitivity coefficients of the temperature with respect to thermal properties k_i, c_{pi}, and h_i for the welded joint shown in Fig. 1.

taken as convective surfaces. In the mechanical analysis the constraints shown in Fig. 3 are applied. Convergence studies were performed by using successively refined grids. The results obtained by the model shown in Fig. 3 were found to be in close agreement with those obtained by finer grids. Typical results are

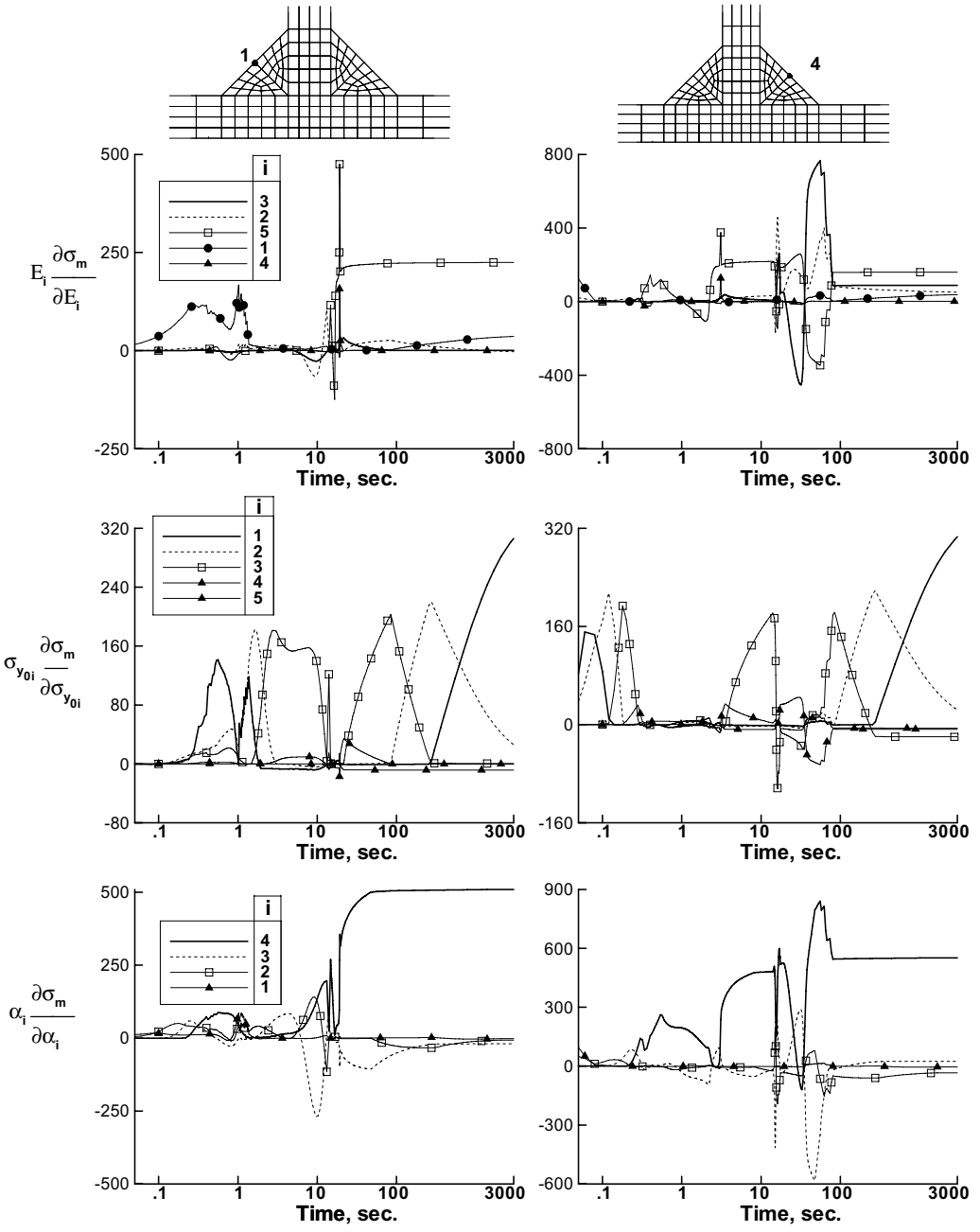

Fig. 7. Time histories of the first-order sensitivity coefficients of von-Mises stress with respect to mechanical properties E_i, σ_{y0i}, and α_i for the welded joint shown in Fig. 1.

shown in Figs. 4 and 5 for the response studies, and in Figs. 6–11 for the sensitivity studies, and are described subsequently.

4.3. Response studies

The time histories of the temperature and von-Mises stress at six points are shown in Fig. 4. The maximum temperatures occur at point 1 at time $t = 14.55$ s, and at point 4 at time $t = 0.55$ s. The maximum

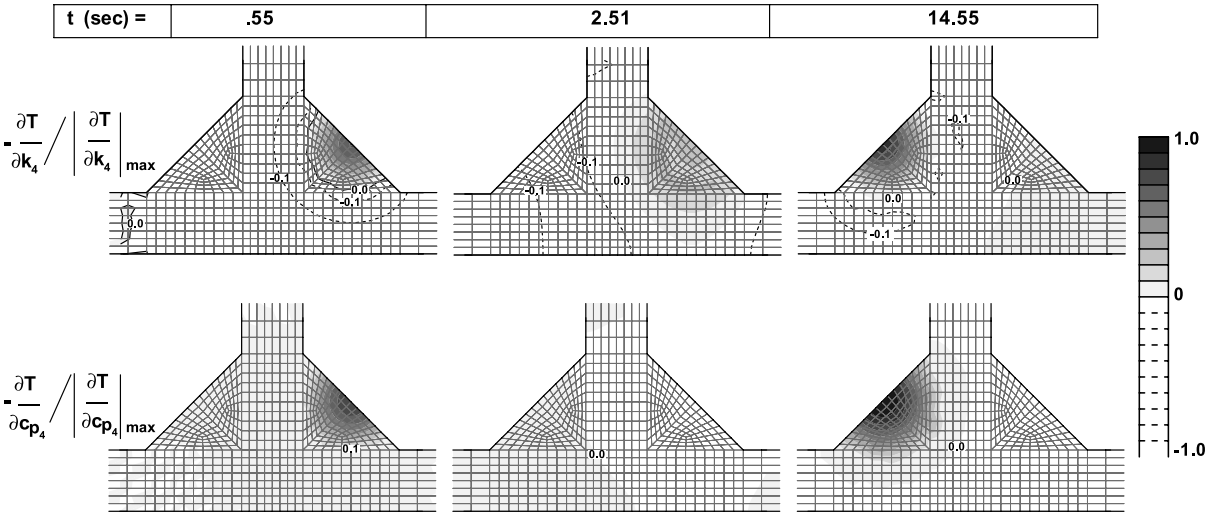

Fig. 8. Snapshots of the first-order sensitivity coefficients of the temperature with respect to thermal properties k_4 and c_{p4} for the welded joint shown in Fig. 1.

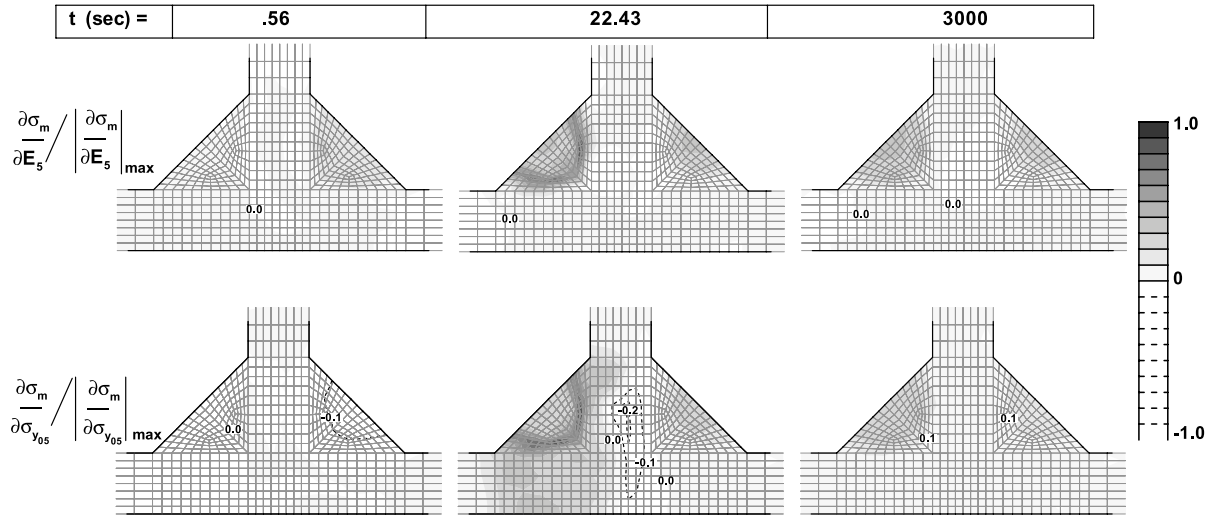

Fig. 9. Snapshots of the first-order sensitivity coefficients of von-Mises stress with respect to mechanical properties E_5 and σ_{y05} for the welded joint shown in Fig. 1.

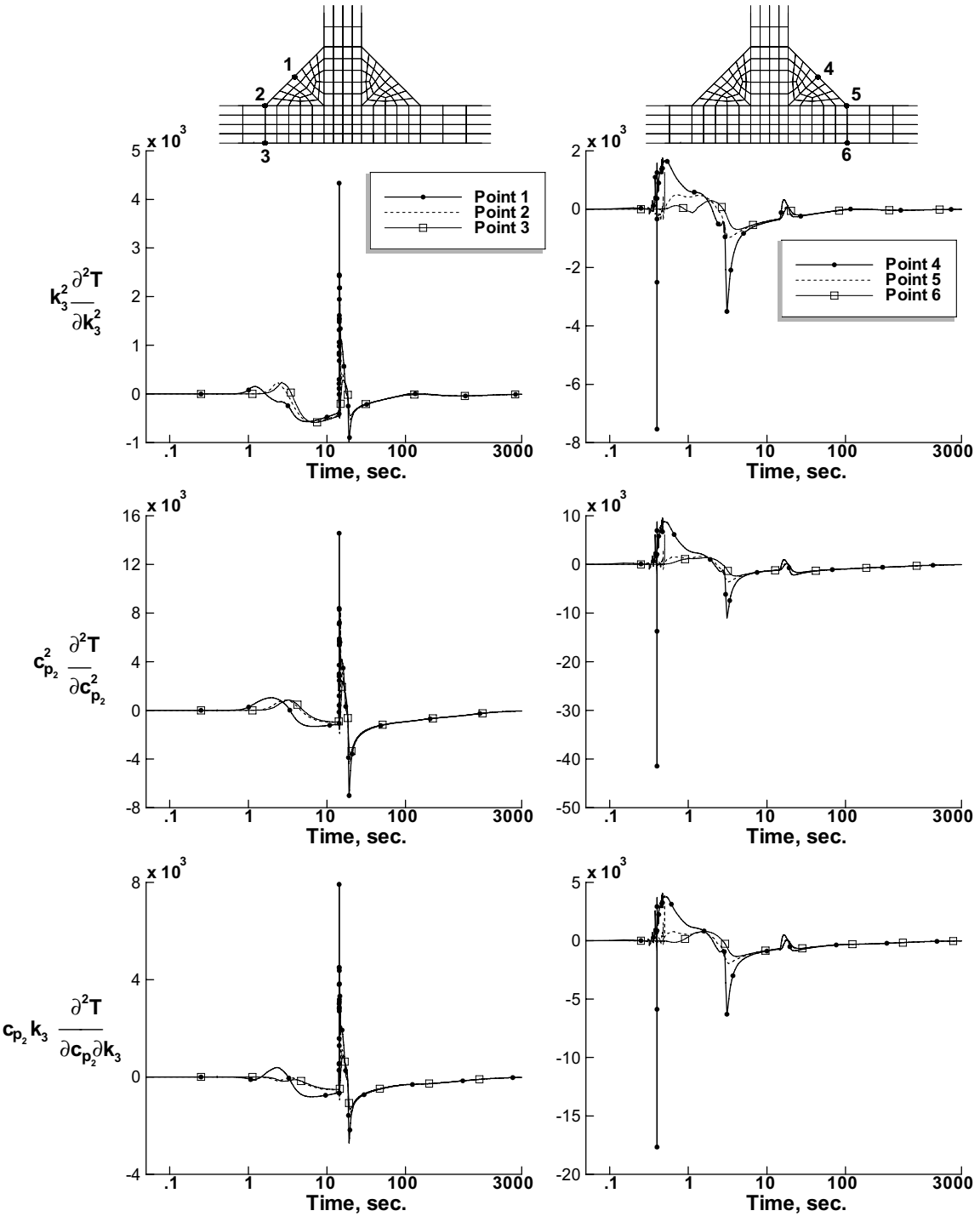

Fig. 10. Time histories of the second-order sensitivity coefficients of the temperature with respect to k_3k_3, $c_{p2}c_{p2}$ and $c_{p2}k_3$ for the welded joint shown in Fig. 1.

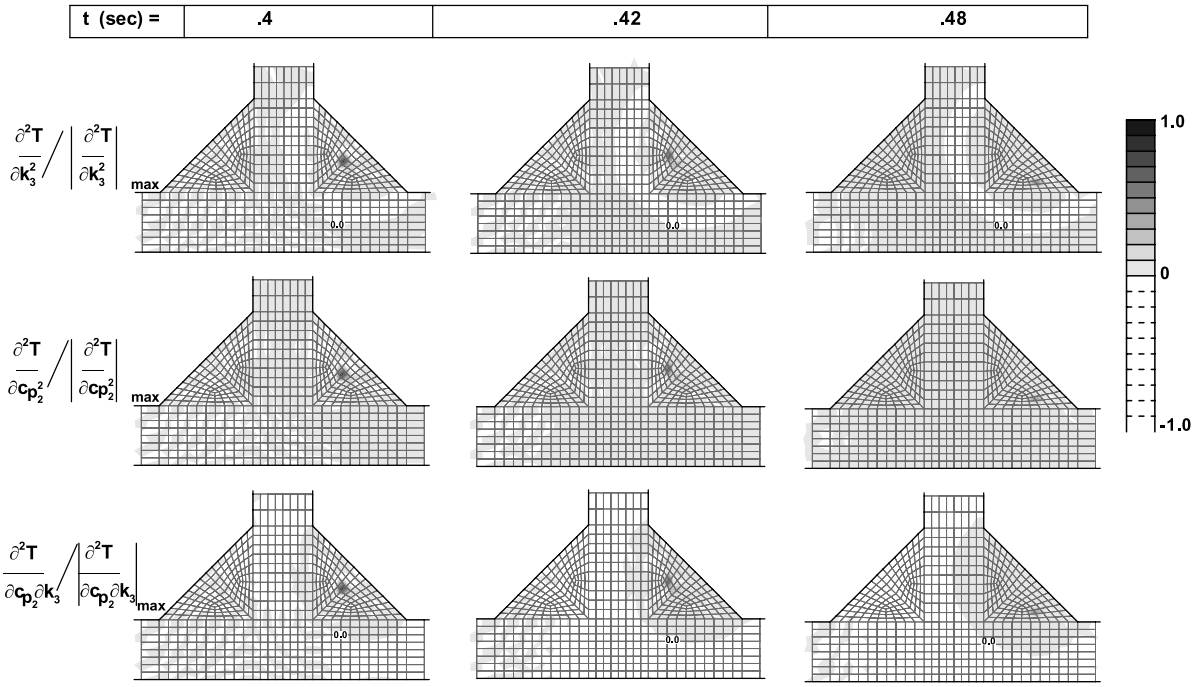

Fig. 11. Snapshots of the second-order sensitivity coefficients of the temperature with respect to k_3k_3, $c_{p2}c_{p2}$ and $c_{p2}k_3$ for the welded joint shown in Fig. 1.

values of the von-Mises stress occur near points 1 and 4 at $t = 3000$ s. Contour plots for the normalized temperature at $t = 0.4$, 0.55 and 14.55 s, and for the von-Mises stress at $t = 0.56$, 14.73, and 3000 s, are shown in Fig. 5. Each contour plot is normalized with respect to the maximum absolute value of the function represented, and consequently the contour intervals are bounded by 0 and 1. An examination of Figs. 4 and 5 reveals that the maximum values of the temperature and von-Mises stress occur in the weld zones.

5. Sensitivity studies

The time histories of the first-order sensitivity coefficients of the temperature with respect to the three sets of parameters k_i, c_{pi}, and h_i at points 1 and 4 are shown in Fig. 6. Corresponding time histories of the first-order sensitivity coefficients of von-Mises stress with respect to the three sets of parameters E_i, σ_{y0i} and α_i at the same points are shown in Fig. 7. Each sensitivity coefficient is normalized by multiplying by the same parameter, with respect to which the sensitivity is evaluated. Contour plots of the largest normalized sensitivity coefficients $\partial T/\partial k_4$ and $\partial T/\partial c_{p4}$ at $t = 0.55$, 2.51 and 14.55 s are shown in Fig. 8. Contour plots for the largest sensitivity coefficients $\partial\sigma_m/\partial E_5$ and $\partial\sigma_m/\partial\sigma_{y05}$ at $t = 0.56$, 22.43 and 3000 s are shown in Fig. 9. Time histories of the largest normalized second-order sensitivity coefficients of the temperature $\partial^2 T/\partial k_3^2$, $\partial^2 T/\partial c_{p2}^2$, and $\partial^2 T/\partial c_{p2}\,\partial k_3$ at six points are shown in Fig. 10. Contour plots of the maximum second-order sensitivity coefficients $\partial^2 T/\partial k_3^2$, and $\partial^2 T/\partial c_{p2}^2$, and of the mixed second-order sensitivity coefficients $\partial^2 T/\partial c_{p2}\,\partial k_3$, at $t = 0.4$, 0.42, 0.48 s are shown in Fig. 11.

An examination of Figs. 5–11 reveals:

1. The first-order sensitivity coefficients of the temperature with respect to the parameters k_4, h_2 and c_{p4} are larger than those with respect to the other parameters in each category.
2. The maximum absolute value of the first-order sensitivity coefficients of T with respect to k_4 and c_{p4} occur at the same point and nearly at the same time as those for T.
3. The first-order sensitivity coefficients of von-Mises stress σ_m with respect to the parameters E_5, σ_{y05}, α_3 and v_1 are larger than those with respect to the corresponding parameters in each category.
4. The maximum absolute values of the first-order sensitivity coefficients of σ_m occur at different points, and at different times from those of T.
5. The second-order sensitivity coefficients of the temperature with respect to k_3 and c_{p2} are larger than the second-order sensitivity coefficients with respect to the corresponding parameters in each category.

6. Concluding remarks

A computational procedure is presented for evaluating the sensitivity coefficients of the quasi-static response of welded structures. Uncoupled thermomechanical analysis is performed. The temperature field is assumed to be independent of stresses and strains. The heat transfer equations emanating from a finite element semi-discretization are integrated using an implicit backward difference scheme to generate the time history of the temperature. The mechanical response during welding is then calculated by solving a generalized plane strain problem. A rate independent, small deformation thermo-elasto-plastic material model with temperature-dependent material properties is adopted in the study.

First- and second-order sensitivity coefficients of the thermal and mechanical response quantities are evaluated by using a direct differentiation approach in conjunction with an automatic differentiation software facility.

Numerical results are presented for a double-fillet conventional welding of a stiffener and a base plate made of stainless steel AL-6XN material. Time histories of the response and sensitivity coefficients, and their spatial distributions at selected times are presented. The first- and second-order sensitivity coefficients can be used to generate taylor series approximations for the quasi-static response for welded joints with slightly different material parameters.

Acknowledgements

The work of J. Song, J. Peters and A. Noor is supported by an Office of Naval Research Grant. The authors acknowledge useful discussions with the grant monitor, Roshdy Barsoum.

References

Argyris, J.H., Szimmat, J., Willam, K.J., 1982. Computational aspects of welding stress analysis. Computer Methods in Applied Mechanics and Engineering 33, 635–666.

Bertram, L.A., Ortega, A.R., 1991. Automated thermomechanical modeling of welds using interface elements for 3D metal deposition. In: Manuscript for Proceedings of ABAQUS User's Conference. Hibbit Karlsson and Sorensen Inc., Oxford.

Bischof, C., Carle, A., Corliss, G., Hovland, P., 1992. Generating derivative codes from Fortran programs. Scientific Programming (1), 1–29.

Bischof, C., Carle, A., Khademi, P., Mauer, A., 1996. Automatic differentiation of FORTRAN. Computational Science and Engineering 3 (3), 18–32.

Braudel, H.J., Abouaf, M., Chenot, J.L., 1986. An implicit and incremental formulation for the solution of elastoplastic problems by the finite element method. Computers and Structures 22 (5), 801–814.

Brown, S., Song, H., 1992. Implications of three-dimensional numerical simulations of welding of large structures. Welding Journal 71 (2), 55s–62s.

Burak, Y.I., Besedina, L.P., Romanchuk, Y.P., Kazimirov, A.A., Morgun, V.P., 1977. Controlling the longitudinal plastic shrinkage of metal during welding. Avt. Svarka 3, 27–29.

Burak, Y.I., Romanchuk, Y.P., Kazimirov, A., Morgun, V.P., 1979. Selection of the optimum fields for preheating plates before welding. Avt. Svarka 5, 5–9.

Carle, A., Fagan, M., Green, L., 1998. Preliminary results from the application of automatic adjoint code generation to CFL3D. AIAA Paper 98-4807.

Chakravati, A.P., Malik, L.M., Goldak, J.A., 1986. Prediction of distortion and residual stresses in panel welds. In: Computer Modelling of Fabrication Processess and Constitutive Behaviour of Metals, Ottawa, Ontario, pp. 547–561.

Connor, L.P. (Ed.), 1987. Welding Handbook, eighth ed. American Welding Society, Miami, FL.

Deo, M.V., Michaleris, P., 2003. Mitigation of welding induced buckling distortion using transient thermal tensioning. Science and Technology in Welding and Joining 8 (1), 49–54.

Goldak, J., Bibby, M., 1988. Computational thermal analysis of welds: current status and future directions. In: Giamei, A.F., Abbaschian, G.J. (Eds.), Modeling of Casting and Weldin Processes IV. The Minerals & Materials Society, Palm Coast, FL, pp. 153–166.

Goldak, J., Chakravarti, A., Bibby, M., 1984. A new finite element model for welding heat sources. Metallurgical Transactions B 15B, 299–305.

Gunnert, R., 1955. Residual Welding Stressed. Almqvist & Wiksell, Stockholm.

Hibbitt, H., Marcal, P.V., 1973. A numerical, thermo-mechanical model for the welding and subsequent loading of a fabricated structure. Computers and Structures 3 (1145–1174), 1145–1174.

Michaleris, P., Tortorelli, D.A., Vidal, C.A., 1995. Analysis and optimization of weakly coupled thermo-elasto-plastic systems with applications to weldment design. International Journal for Numerical Methods in Engineering 38 (8), 2471–2500.

Oddy, A.S., Goldak, A.J., 1990. Consistent strain fields in 3d finite element analysis of welds. ASME Journal of Pressure Vessel Technology 112 (3), 309–311.

Roelens, J.B., Maltrud, F., 1993. Determination of residual stresses in submerged arc multi-pass welds by means of numerical simulation and comparison with experimental measurements. In: IIW Annual Assembly, Glasgow, Doc. X-1279.

Rybicki, E.F., Stonesifer, R.B., 1979. Computation of residual stresses due to multipass welds in piping systems. Journal of Pressure Vessel Technology 101, 149–154.

Saltelli, A., Chan, K., Scott, E.M. (Eds.), 2000. Sensitivity Analysis. John Wiley & Sons, Inc., Hoboken, NJ.

Shim, Y., Feng, Z., Lee, S., Kim, D., Jaeger, J., Paparitan, J.C., Tsai, C.L., 1992. Determination of residual stress in thick-section weldments. Welding Journal 71, 305s–312s.

Simo, J.C., Taylor, R.L., 1985. Consistent tangent operators for rate-independent elasto-plasticity. Computer Methods in Applied Mechanics and Engineering 48, 101–118.

Tekriwal, P., Mazumder, J., 1991. Transient and residual thermal strain–stress analysis of GMAW. Journal of Engineering Materials and Technology 113, 336–343.

Terai, K., 1978. Study on prevention of welding deformation in thin-skin plate structures. Technical Report 61, Kawasaki.

Wang, J., Murakawa, H., 1998. A 3-d fem analysis of buckling distortion during welding in thin plate. In: 5th International Conference in Trends in Welding Research, Pine Mountain, GA.